

Theoretical Insights into the Role of Lattice Fluctuations on the Excited Behavior of Lead Halide Perovskites

Yoonjae Park, Rohit Rana, Daniel Chabeda, Eran Rabani, and David T. Limmer*



Cite This: <https://doi.org/10.1021/accountsmr.4c00401>



Read Online

ACCESS |

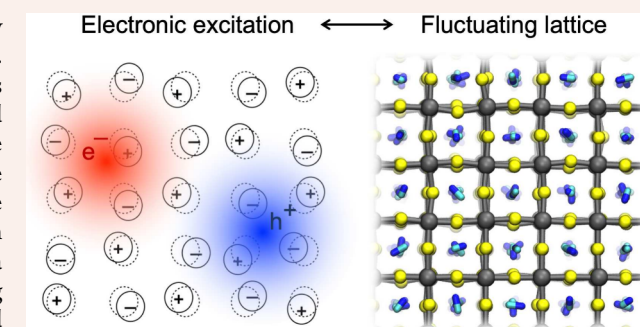
Metrics & More

Article Recommendations

CONSPECTUS: Lead halide perovskites have been extensively studied as a class of materials with unique optoelectronic properties. A fundamental aspect that governs optical and electronic behaviors within these materials is the intricate coupling between charges and their surrounding lattice. Unravelling the role of charge-lattice interactions in the optoelectronic properties in lead halide perovskites is necessary to understand their photophysics. Unlike traditional semiconductors where a harmonic approximation often suffices to capture lattice fluctuations, lead halide perovskites have a significant anharmonicity attributed to the rocking and tilting motions of the inorganic framework. Thus, while there is broad consensus on the importance of the structural deformations and polar fluctuations on the behavior of charge carriers and quasiparticles, the strongly anharmonic nature of these fluctuations and their strong interactions render theoretical descriptions of lead halide perovskites challenging. In this Account, we review our recent efforts to understand how the soft, polar lattice of this class of materials alters their excited state properties. We highlight the influence of the lattice on static properties by examining the quasiparticle binding energies and fine structure. With perovskite nanocrystals, we discuss how incorporating lattice distortion is essential for accurately defining the exciton fine structure. By considering lattices across various dimensionalities, we are able to illustrate that the energetics of excitons and their complexes are significantly modulated by polaron formation. Beyond energetics, we also delve into how the lattice impacts the dynamic properties of quasi-particles. The mobilities of charge carriers are studied with various charge-lattice coupling models, and the recombination rate calculation demonstrates the molecular origin on the peculiar feature in the lifetime of charge carriers in these materials. In addition, we address how lattice vibrations themselves relax upon excitation from charge-lattice coupling. Throughout, these examples are aimed at characterizing the interplay between lattice fluctuations and optoelectronic properties of lead halide perovskites and are reviewed in the context of the effective models we have built and the novel theoretical methods we have developed to understand bulk crystalline materials, as well as nanostructures and lower dimensionality lattices. By integrating theoretical advances with experimental observations, the perspective we detail in this Account provides a comprehensive picture that serves as both design principles for optoelectronic materials and a set of theoretical tools to study them when charge-lattice interactions are important. These insights may further guide the development of next-generation optoelectronic devices with improved efficiency and stability while also inspiring new research directions to explore emerging quantum phenomena in these materials.

I. INTRODUCTION

Over the past 20 years, lead halide perovskites have emerged as important materials for a variety of photovoltaic and light-emitting applications. On top of their ease of synthesis, tunable optoelectronic properties and high defect tolerance,^{1–3} they have small exciton binding energies,⁴ long carrier lifetimes and diffusion lengths⁵ despite modest charge mobilities,⁶ and have demonstrated high power conversion efficiencies and quantum yields. Consisting of a lead-halide inorganic framework and counterbalancing cations, lead halide perovskites are held together with ionic bonds that localize significant charge leading to strong Coulomb interactions between photoexcited carriers and the surrounding lattice.⁷ The isotropic nature of



this ionic bonding results in a deformable lattice, admitting structural fluctuations and polaron formation that can protect charges from scattering with defects,^{8,9} and screen the interaction between charges.¹⁰ Although many of the important optical properties in perovskites are presumed to

Received: June 17, 2025

Revised: September 12, 2025

Accepted: September 21, 2025

arise from the interplay of electronic structure and charge-lattice interactions,^{2,11} elucidating their microscopic origin has remained challenging.

The significant anharmonicity of perovskite lattices means that traditional models and perspectives on electron–phonon coupling are not appropriate. Unlike most crystalline semiconducting materials where lattice fluctuations are well described by a harmonic approximation, perovskites have rocking and tilting motions of the inorganic framework that are better described by double well potentials, and they exhibit nearly free motions of their A-site cations.² Unsurprisingly, these soft modes produce a number of competing structural phases that can be accessed over typical operating conditions or tuned through nanocrystalline size. In lower dimensional crystals, the A-site cation can be replaced with ionic ligands, which themselves can disorder and admit large fluctuations.¹² Even at low temperatures, where a harmonic approximation may be valid, perovskites have complex unit cells, rendering the use of traditional theoretical methods computationally intractable. There have been a growing number of studies pointing to the importance of charge-lattice effects on the properties of lead-halide perovskites, motivating analytical¹³ and numerical studies.^{13,14} *Ab initio* based approaches have been widely developed; however, they are often difficult to extend to the time and length scales necessary to capture the complex interplay between lattice fluctuations and charge carriers in perovskites and further limited by the range of coupling strength they can treat. Balancing an atomistic description of the lattice and a nonperturbative treatment of charge-lattice coupling has therefore required that novel theoretical techniques be developed. To address this, we have developed path integral based methods, which incorporate the full quantum statistical behavior of light quantum particles, in order to describe charge-lattice effects nonperturbatively,^{15,16} and adapted pseudopotential methods¹⁷ to study nanocrystals and the role of surface relaxation on quasiparticle energetics and lifetimes.¹⁸ These tools have enabled studies on exciton binding and charge carrier renormalization from polaron formation and an elucidation of the interplay between lattice structure and exciton energies in nanomaterials.

In this Account, we summarize these theoretical developments and how they have been used to rationalize spectroscopic and excited state dynamics in these material systems. Section II presents a discussion on static properties of excited states focusing on exciton fine structure and binding energies of excitons and biexcitons and how each depends on the lattice geometry and particle morphology. We continue in Sec. III by addressing how the lattice fluctuations alter the dynamic properties such as charge mobility and the lifetimes of charge and lattice excitations. In each subsection, we specify the types of perovskites considered, ranging from zero-dimensional nanocrystals to their three-dimensional bulk counterparts. In Sec. IV, we conclude this with a summary and active areas of continued study.

II. STATIC PROPERTIES

The generation, dissociation, and recombination of excitons determine the power conversion efficiencies and quantum yields of the devices. The energetics of excitons and other quasiparticle excitations offer figures of merit for designing semiconducting materials as they correlate with relevant dynamical properties. Details of these static properties and how they depend on the static or evolving lattice are reviewed

here. In particular, we review (i) how lattice distortion influences exciton fine structure in nanocrystals and (ii) how the binding energies of excitons and their complexes are modulated by confinement and polaronic effects.

II.A. Exciton Fine Structure

Lead halide perovskite nanocrystals are considered a promising quantum light source material as they show a remarkable brightness for photoluminescence and high quantum yield.¹⁹ The origin of the bright emission has been a subject of debate, since there are conflicting experimental reports on the nature of the excitonic ground state, and the size of the dark-bright excitonic spittings.^{20,21} The excitonic fine structure of a material can be inferred, in principle, from spectroscopic measurements at cryogenic temperatures, though such measurements are challenging. While in bulk semiconductors the splitting of dark-bright exciton sublevels is very small, the splitting in nanocrystals can be substantial.

For materials with strong spin–orbit coupling like the lead halide perovskites, spin and angular momentum are correlated, resulting in a spin–lattice coupling that can change and possibly invert the spitting of optically bright and dark states. In the bulk, lead halide perovskites undergo structural phase transitions between low temperature orthorhombic phases, intermediate tetragonal phases, and high temperature cubic phases, each with different symmetry and thus changes to the electronic band structure.²³ In nanoparticles, the locations of phase transformations are generally at different temperatures than their bulk counterparts, and their significant surface-to-volume ratios can result in further complications as those surfaces relax and reconstruct.

Using an atomistic force field,²⁴ we studied a series of CsPbI₃ perovskite nanocrystals whose relaxed structures are shown in Figure 1(a). We observed that the local lattice structure was size-dependent, with the smallest nanocrystals stabilizing a highly symmetric cubic phase, whereas the largest ones recovered a bulk-like orthorhombic structure. The degree of asymmetry was quantified in Figure 1(b), using a lattice anisotropy parameter defined as the difference in the Pb–Pb distance between shortest and longest axis of the nanocrystal. The values for cubic structures are zero, and for orthorhombic structures, the tilting of the octahedra breaks the isotropic symmetry, resulting in a small constant value of the order parameter. This work found that the relaxed structures did not monotonically transition between cubic and orthorhombic with increasing size and rather exhibit a maximum anisotropy for cubes with edge lengths of 2.7 nm. These observations were broadly consistent with experimental X-ray measurements.¹⁸ This size dependence stems from the competition between surface relaxation and the stability of the bulk orthorhombic phase. The establishment of the nanoparticle structure was only theoretically tractable with *ab initio* derived force fields, as it is computationally intractable to relax geometries directly with density functional theory for such large systems.

The exciton fine structures were subsequently obtained from semiempirical pseudopotential methods¹⁷ using the Bethe-Salpeter equation²⁵ developed in ref.²² on the geometries obtained from the force field calculations. The electronic pseudopotentials were parametrized to include both the effect from lattice distortion and spin–orbit coupling. Only with such a theoretical framework could the correlated electronic structure of the nanoparticles be computed. With this methodology, we found the excitonic ground state to be

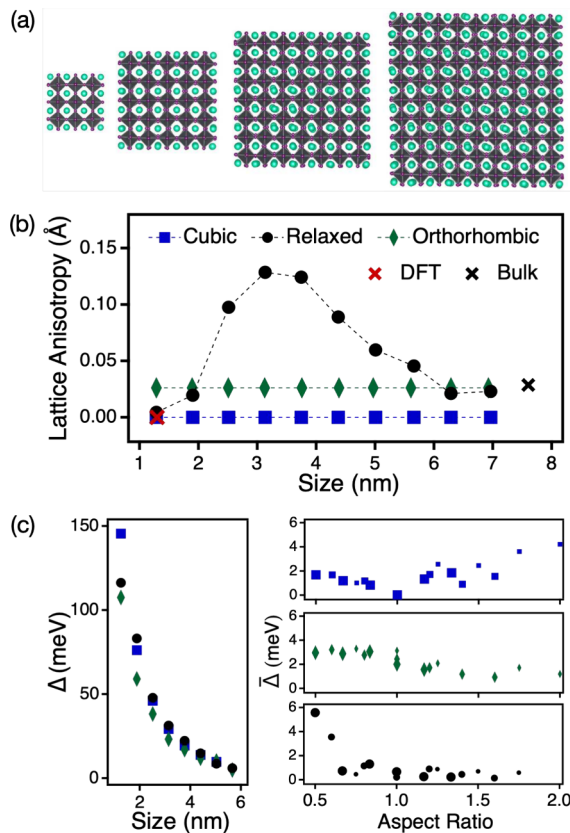


Figure 1. (a) Relaxed structures of CsPbI₃ perovskite nanocrystals for the size of 1.9, 3.1, 4.4, and 5.7 nm, where I and Cs atoms are shown in purple and teal with gray Pb octahedra. (b) The lattice anisotropy parameter for cubic (blue squares), relaxed (black circles), and orthorhombic (green diamonds) structures. Red and black \times symbols indicate the results from DFT and Bulk perovskite. (c) The splittings, Δ , between dark and bright excitonic states with various nanocrystal sizes (left) and the standard deviation of splittings, $\bar{\Delta}$, between bright excitonic states as a function of aspect ratio (right) for cubic (blue), orthorhombic (green), and relaxed crystal structures (black). Reproduced with permission from ref 22. Copyright 2023 American Chemical Society.

dark with spin triplet character, exhibiting a small Rashba coupling, which is implied by the similar splitting trends as increasing nanocrystal sizes for all phases shown in Figure 1(c, left). For cubic phases of cubic nanoparticles, the three bright states are degenerate, but deviations locally in the unit cell or morphologically in the aspect ratio of the nanocrystal could break this degeneracy. With the relaxed structure of each nanocrystal, Figure 1(c, right panels) describes the standard deviation $\bar{\Delta}$ of splittings between bright excitonic states as a function of the aspect ratio. Unlike the cubic and orthorhombic structures, the splittings with low aspect ratio are significant, unique feature of relaxed structures. This study confirmed that the lattice symmetry is vital in interpreting exciton fine structure of perovskite nanocrystals.

II.B. Exciton Binding Energy in Bulk

While the absolute energies of excitons determine what states are populated thermally, the exciton binding energy marks the threshold to generate free charge carriers from an initial photoexcitation and determines the relative proportion of bound excitons to free charge carriers. Bulk lead-halide perovskites have shown anomalously small values for exciton

binding energies, typically reported as less than thermal energy at room temperature, attracting a great attention as a promising material for photovoltaic applications.⁴ First principle estimates of exciton binding energies had failed to recover the anomalously small exciton binding energies,²⁶ and while simple effective mass models could be made consistent with experiments, they typically required values of the dielectric constants that were difficult to interpret.²⁷ The difficulty in establishing the exciton binding energy from such studies implicated the role of exciton-polarons and lattice deformation in the renormalization of the observed binding energies. Such effects are not often accounted for in solid-state electronic structure.

The approach developed in this work was based on imaginary time path integrals^{31–34} using an explicit atomistic representation of the lattice. Perovskites have highly dispersive bands, so the low energy band structure is well described by effective mass models. The lattice Hamiltonian was given by the previously validated atomistic force field³⁵ and the charge-lattice coupling was described by the sum of pseudopotentials,^{15,16} in which way all orders of anharmonic features of perovskite lattice can be captured. Within this model, imaginary time path integrals could then be used to treat electron–hole correlation and charge-lattice coupling without resorting to perturbation theory or approximate analytical results.

We found good agreement with most experimental reports for exciton binding in the methylammonium lead-iodide perovskites, MAPbI₃, establishing a binding energy of 21 meV. The lattice renormalization of exciton binding occurs through two mechanisms, as illustrated in Figure 2(a). First,

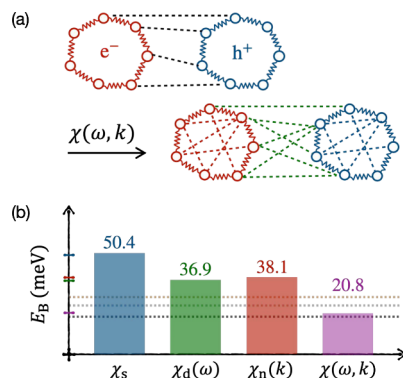


Figure 2. (a) Illustration of two mechanisms describing how exciton binding energy is renormalized by the lattice. Reproduced with permission from ref 16. Copyright 2022 AIP Publishing LLC. (b) Exciton binding energy, E_B , computed under different types of lattice screenings where dotted lines indicate experimental values from ref 28 (black), ref 29 (gray), and ref 30 (brown). Reproduced with permission from ref 15. Copyright 2022 American Chemical Society.

the lattice screens the direct interaction between charges by the static dielectric constant. This is a direct effect, weakening the Coulomb potential between the electron and hole. Second, the lattice stabilizes the free charges, altering their and the exciton's self-energy. This effect reflects in polaron formation of free charges or exciton-polaron formation of the bound electron–hole pair. This work found that exciton-polaron binding energies are relatively small, as a charge neutral object couples weakly to the lattice, but the stabilization of both the electron

and hole from polaron formation is significant, and directly responsible for the attenuation of the binding energy.

We developed an effective field theory to decompose the contribution from the lattice on excitonic properties,¹⁵ through different approximations to the lattice Green's function, $\chi(k, \omega)$. In principle, $\chi(k, \omega)$ includes both a frequency, ω and wavevector, k , dependence. In a *static* screening model, the electron–hole interaction is only screened by an effective dielectric constant, ignoring the dependence on both ω and k , $\chi(k, \omega) \approx \chi_s$. In a *dynamic* screening model, we could incorporate the effect from harmonic phonons through a Fröhlich-like model^{8,36} for a charge that is coupled with polarization field produced from the collective harmonic motions of the lattice. The models in this approximation were dispersionless, so $\chi(k, \omega) \approx \chi_d(\omega)$, but whose frequency dependence admits the formation of a polaron through the quantum mechanical treatment of the lattice. Alternatively, a *nonlocal* screening model with a spatially dependent dielectric function from the explicit MAPbI_3 lattice, $\chi(k, \omega) \approx \chi_n(k)$, was developed. In this model, the frequency dependence was ignored, which is equivalent to assuming it is well-described classically. The computed exciton binding energy under each type of lattice screening is summarized in Figure 2(b), including the full lattice Green's function that incorporates both nonlocality and frequency dependence. Comparisons show that the inclusion of lattice effects from either dynamic or nonlocal screening reduces the attraction between electron and hole by about 10 meV, but incorporating both of these effects provides an excellent agreement with experiments, accounting for a nearly 30 meV red shift of the binding energy (21 meV) compared to the simple effective mass estimate (50 meV).³⁷ This clarified the origin of the small exciton binding energy, emphasizing the importance of anharmonic lattice fluctuations and polaron formation in lead halide perovskites. With more accurate experimental data to parametrize the Fröhlich model, and more consistent determination of its coupling constant, perhaps even better agreement can be found.

II.C. Exciton Binding in Two-Dimensions

Two-dimensional layered hybrid organic–inorganic perovskites have been proposed as alternatives to their bulk counterparts due to enhanced tunability and stability.⁴² Consequently, the photophysics of two-dimensional perovskites is different than that of bulk perovskites. The heterogeneous layer composition leads to a dielectric contrast that enhances the electron–hole interaction.⁴³ The electron–hole interaction is also enhanced by quantum confinement that arises from the exciton and inorganic layer length-scales being similar in value.⁴³ However, it remains to be understood how excitons are renormalized due to charge-phonon interactions in two-dimensional perovskites. To approach this problem, we considered two model systems with organic ligands, n -butylammonium (BTA) and phenylethylammonium (PEA), $(\text{BTA})_2(\text{MA})_{n-1}\text{Pb}_n\text{I}_{3n+1}$ and $(\text{PEA})_2(\text{MA})_{n-1}\text{Pb}_n\text{I}_{3n+1}$ where n is the number of inorganic sublayers. A change in n corresponds directly to a change in the quantum well thickness, thus also modifying the confinement. We studied both crystals formed from alternating slabs of organic and inorganic material, as well as single sheets dispersed in solution, the latter of which is reported in Figure 3.

To study the renormalization to exciton binding in these model systems and geometries, we developed a path integral framework⁴¹ similar to the one used to investigate bulk

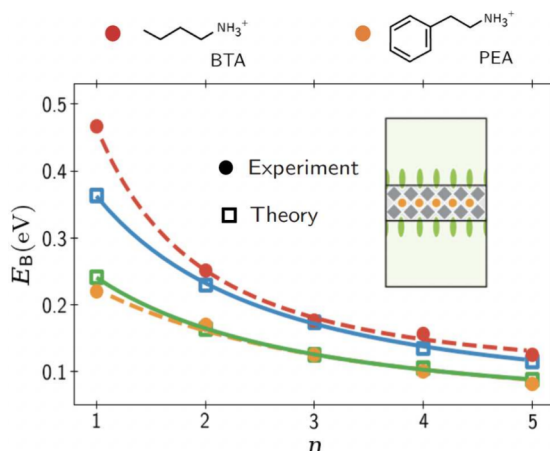


Figure 3. Exciton binding energies for thin slab geometries, illustrated in the inset, for both $(\text{BTA})_2(\text{MA})_{n-1}\text{Pb}_n\text{I}_{3n+1}$ (red and blue) and $(\text{PEA})_2(\text{MA})_{n-1}\text{Pb}_n\text{I}_{3n+1}$ (orange and green). Circles are experimental data from refs 38–40, and squares are from theoretical calculations from ref 41. Lines are guides for the eye. Reproduced with permission from ref 41. Copyright 2025 American Chemical Society.

perovskites. Specifically, we employed continuum electrostatics along with the thin-film Fröhlich interaction derived for a thin-film geometry.⁴⁴ Figure 3 shows that the inclusion of a dynamic lattice brings exciton binding energies in reasonable agreement with experiment for both materials.^{38–40} The binding energy for the BTA ligand is much larger than that for the PEA ligand due to the large dielectric contrast between the organic layer and the inorganic lattice. Both exhibited a strong dependence on n , illustrating the effect of dielectric confinement. When studying the polaron, we observed a nonmonotonic behavior of polaron binding energy as a function of quantum well thickness n . We were able to capture this nonmonotonic trend with a variational bound that has two length scales: one that corresponds to an effective dielectric screening radius and another that corresponds to the polaron radius.⁴¹ To physically rationalize this trend, we consider two competing mechanisms. The first is that as n increases, the amount of polar inorganic material increases, thus leading us to expect the electron–phonon interaction to strengthen. The second is that as n increases, a lattice dipole becomes weakened due to stronger screening from the inorganic layer, thus leading us to expect the electron–phonon interaction to weaken. Overall, we were able to elucidate the interplay among quantum confinement, dielectric confinement, and charge-phonon coupling in two-dimensional perovskites.

II.D. Biexciton Binding in Cubic Nanocrystals

While there is reasonable agreement on the size of exciton binding energies in bulk perovskites, the values for perovskite nanocrystals are comparatively less established, and the understanding of multiparticle energies is even more unclear. In nanocrystals, quantum confinement can lead to strong many-body interactions among photoexcited charges and these can significantly affect the optical properties,⁴⁵ implying that it is necessary to study the behavior of exciton complexes such as biexcitons. Recently, experimental studies⁴⁶ proposed an antibinding behavior of biexcitons in CsPbBr_3 nanocrystals, implicating the potential lattice effect on these interactions. A number of biexciton binding energies for lead halide perovskites have been reported to date, whose values span a wide range even with opposite signs.^{45,46} However, exper-

imental analysis is difficult because of effects from thermal broadening, spectral drifts, and the large variance in the nanocrystal sizes.⁴⁷

Adopting an analogous path integral approach as employed to study other perovskite systems, the energetics of quasiparticle excitations in CsPbBr_3 perovskite nanocrystals are reviewed⁵⁰ where Figure 4(a) shows the snapshots of

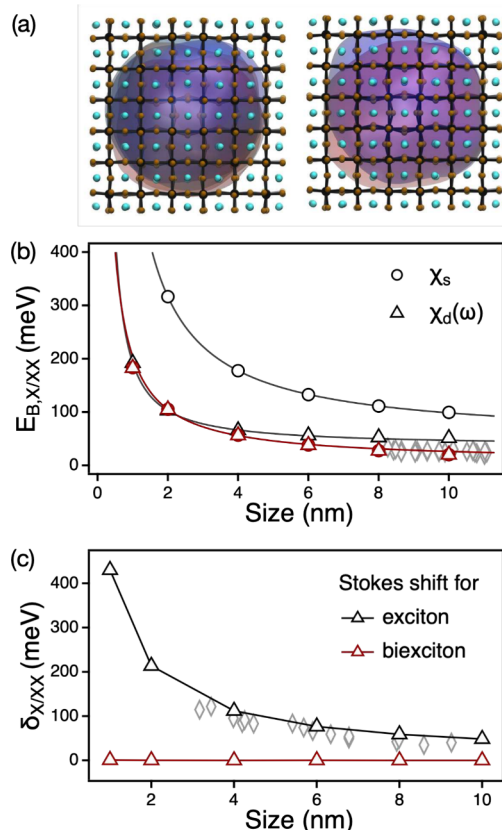


Figure 4. (a) Simulation snapshot of biexciton (left) and exciton (right) interacting with CsPbBr_3 perovskite nanocrystal with 3.56 nm as the edge length of the nanocrystal. Electrons and holes are represented as red and blue ring polymers. (b) Exciton ($E_{B,\text{exc}}$, black) and biexciton ($E_{B,\text{biex}}$, red) binding energies over the range of nanocrystal sizes where results from static and dynamic lattice screenings are shown with circles and triangles, respectively. Solid lines are fitted lines. (c) The difference in exciton (δ_{exc} , black) and biexciton (δ_{biex} , red) binding energies from static screening, implying the values of the Stokes shift. Solid line is a guide to the eye. Gray diamond symbols indicate experimental measurements reported by Cho et al.⁴⁸ in panel (b) and Brennan et al.⁴⁹ in panel (c), respectively, providing additional support for the validity of theoretical models. Reproduced with permission from ref 50. Copyright 2023 American Physical Society.

molecular dynamics simulations of biexciton and exciton in CsPbBr_3 nanocrystal with electrons and holes represented as imaginary time paths under the external potential accounting for a dielectric confinement effects. For comparison, the static and dynamic lattice screening models noted above are also considered, together with explicit electron–hole correlation. Over the range of nanocrystal sizes, exciton and biexciton binding energy calculations were performed under each type of lattice screening. Shown in Figure 4(c) is the difference in exciton and biexciton binding energies compared with results from static screening model. Even with the strong size

dependence of both exciton and biexciton binding energies, the large values of δ_x imply that the inclusion of lattice effects either from dynamic or explicit CsPbBr_3 lattice screening largely suppresses the exciton binding energy, whereas lattice effects are negligible for biexciton binding. This observation is rationalized by the mechanism of polaron formation where instead of weakening the electron–hole interaction, lowering the self-energies of free charges contributes dominantly to reducing the binding energies in nanocrystals, which is not relevant for biexciton binding energies. Further, despite ongoing debate over the wide range of reported experimental values, the calculations on biexciton binding energies are in agreement with other size-dependent measurements on CsPbBr_3 nanocubes,⁴⁸ and confirm that biexcitons are bound for all nanocrystal sizes considered, regardless of the type of lattice screenings.

III. DYNAMIC PROPERTIES

The dynamics of charges and the surrounding lattice play a crucial role in the functioning of semiconductor based devices. After photoexcitation, the subsequent relaxation dynamics involves a number of different processes which occur on time scales that span the picoseconds of exciton dissociation and lattice vibration to nano- and microseconds for charge carrier lifetimes all of which conspire to determine a device's efficiency. Establishing a microscopic understanding of these processes and how each is influenced by the soft, polar lattice provides means of designing materials to optimize optoelectronic properties. In this section, we focus on how lattice fluctuations alter the diffusion and lifetimes of charge carriers as well as the lifetimes of lattice vibrations.

III.A. Charge Carrier Mobility

In the application of semiconducting materials, the mobility of charge carriers is one of primary properties that limits the performance of materials. In photovoltaic devices, free charge carriers need to reach the extraction layer within their lifetime to make use of them whereas in light-emitting devices, larger mobility implies the greater brightness with low driving voltage.⁵¹ Experimentally, the relative carrier mobility can be extracted from the photoinduced conductivity measurement using the pump–probe THz transmission dynamics after photoexcitation where the intensity of the signal is proportional to the density of free charge carriers.⁶ Studying charge transport phenomena in lead halide perovskites, Wehrenfennig et al. showed that the difference in charge mobility highly affects the performance of materials.⁶ Charge lattice interactions and polaronic effects in particular have been implicated in observations of renormalizing charge mobilities, as scattering off of the lattice is the primary mechanism of dissipation for excess charges.¹⁴

Using our quasiparticle path integral approach,^{31–34} we have estimated the relative charge carrier mobility at various electron–phonon coupling strengths using Fröhlich model Hamiltonian.^{8,36} In the antiadiabatic limit which is applicable to lead halide perovskites, the charge mobility μ can be obtained from their renormalized mass m^* as⁵²

$$\mu = \frac{e}{2\alpha\omega m^*} e^{\beta\hbar\omega} \quad (1)$$

where ω is a longitudinal optical frequency of phonons, α is a dimensionless Fröhlich coupling constant, β is inverse temperature times Boltzmann's constant and \hbar is Planck's

constant. An inverse renormalized mass at a given electron–phonon coupling strength can be computed using a linear response relation⁵³

$$\frac{1}{m^*} = \lim_{\beta \rightarrow \infty} \frac{\langle (\Delta r)^2 \rangle}{3\beta \hbar^2} \quad (2)$$

where Δr is the distance between the first and the last beads of an open-chain imaginary time path, pictorially shown in Figure 5(a).

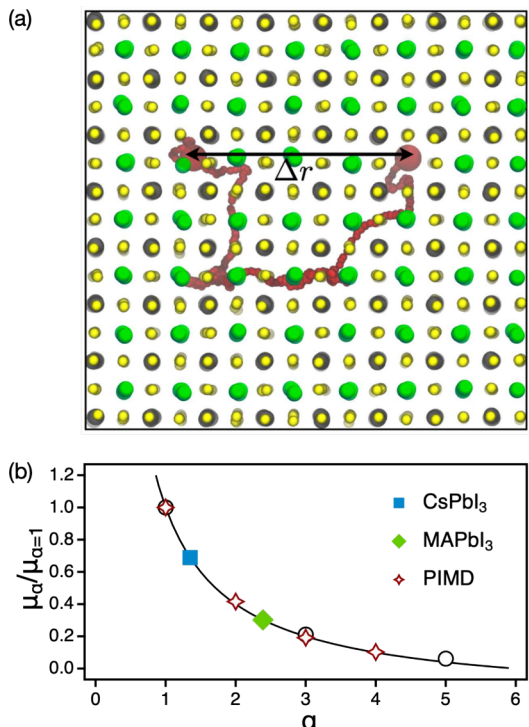


Figure 5. (a) Schematic of how to evaluate effective mass from an open-chain imaginary time path. (b) The relative charge mobilities μ obtained from effective masses at various electron-coupling strength α in CsPbI₃ and MAPbI₃ perovskites with results from the path integral approach. Solid line represents the estimate from Feynman's variational method.

Adopting the material properties of bulk lead-halide perovskites, the relative charge mobilities are described in Figure 5(b), at various electron–phonon coupling strengths. In this parameter regime, the effective mass is well described using first order perturbation theory⁹ and is consistent with Feynman's variational method.⁵⁴ Combining these two results, we were able to infer that the coupling with phonons makes the charge carriers heavier while suppressing the carrier mobility, with a greater reduction expected for MAPbI₃ compared to CsPbI₃ due to its smaller Fröhlich coupling constant. Molecularly, the weaker charge-lattice coupling for the inorganic lattice originates in the slightly less polarizable A-site cation.

III.B. Electron–Hole Recombination Rate

At typical operating conditions for bulk photovoltaics, electron–hole recombination determines the lifetimes of charge carriers. Despite their modest mobilities, the lead halide perovskites exhibit large diffusion lengths, enabling exceptions of power conversion efficiencies. Over the past decade, it has been found that the origin of the large diffusion

lengths is an abnormally long free carrier lifetime, or correspondingly low radiative recombination rate.⁵ It had been conjectured that polaronic effects play a major role in the underlying mechanism of low electron–hole recombination rates of perovskites,^{1,10} though direct evidence theoretically or experimentally had been lacking. We were able to elucidate the molecular origin of the long charge carrier lifetime as originating from an emergent repulsion between electrons and holes mediated by the soft perovskite lattice.

In general, the charge recombination rate in the bulk is understood using a bimolecular rate expression.⁶ For the reaction of $e^- + h^+ \rightarrow \hbar\nu$, the bimolecular recombination rate k_r can be defined as

$$\frac{dn_e}{dt} = -k_r n_e n_h \quad (3)$$

where $n_{e/h}$ is the electron/hole density. We used quasiparticle path integral molecular dynamics simulations with an atomistic description of the MAPbI₃ lattice to evaluate this rate. In a bulk system, recombination is a bimolecular process, so the rate is proportional to the probability of bound electron and hole being colocalized, and a conditional probability of radiating provided they are colocalized.^{15,16} Both depend on the effective potential between charges, as mediated through a finite temperature and fluctuating lattice. Using explicit simulations, we found at 300 K a nonlocal lattice Green's function, $\chi_n(k)$, was well approximated by

$$\chi(k) = \frac{\chi_0}{1 - l_s^2 k^2 + l_c^2 l_s^2 k^4} \quad (4)$$

characterized by two length scales, l_s and l_c which are screening and correlation lengths associated with dielectric fluctuations. This functional form includes a single resonant peak that results from the double well potential of the optical mode.¹³

As the lattice Green's function screens in the electron–hole interaction, in the limit that the lattice is well described classically, it implies an effective potential

$$V(r) = -\frac{e^2}{4\pi\epsilon_0 r} \left[\frac{1}{\epsilon_\infty} + \frac{1}{\epsilon^*} + \frac{\gamma}{4\delta\epsilon^*} e^{-r\delta} \sin[r\gamma - \theta] \right] \quad (5)$$

where r is the distance between two charges, $1/\epsilon^* = \chi_0 \alpha^2 \epsilon_0 / e^2$, $\gamma^{-1} \approx \sqrt{2} l_c$, $\delta^{-1} \approx 2l_c / \sqrt{1 - l_s/2l_c}$, and $\theta = \arctan[2\delta/\gamma]$. Notably this potential, shown in Figure 6(a), includes a barrier at intermediate distances. This electron–hole repulsion significantly decreases their wave function overlap relative to expectations without a fluctuating lattice, χ_s , or within its dispersionless harmonic approximation, χ_d . All three approximations to the screening from the lattice are shown in Figure 6(b) where the electron–hole radial probability density is plotted, $p(r)$. Under standard approximations using either the static or harmonic approximation, the expected lifetimes of charge carriers at concentrations $n_e = 10^{17}/\text{cm}^3$ are on the order of $1/k_r n_e \approx 10$ ns, while it rises to $1/k_r n_e \approx 200$ ns when the nonlocal screening from the lattice is taken into account. This latter estimate was in very good agreement with photoluminescence lifetime measurements under similar carrier concentrations.^{4,5} This study thus resolved the longstanding question concerning the anomalously long carrier lifetimes by invoking a novel lattice mediated repulsion. This mechanism was molecular in origin, as reflective in the length scales l_s and l_c .

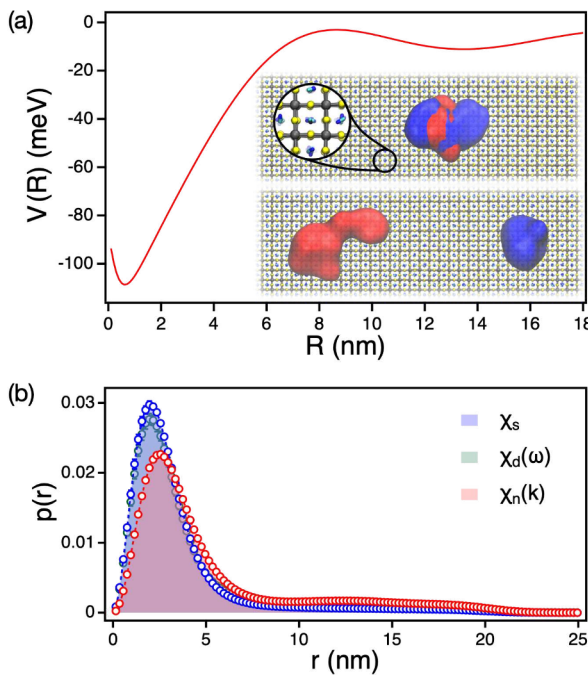


Figure 6. (a) An effective potential obtained from the free energy between electron and hole in MAPbI_3 perovskite as a function of the distance between centroids of quasiparticles. The inset is the representative snapshots of molecular dynamics simulations of electron (red) and hole (blue) with the MAPbI_3 lattice where Pb^{2+} , I^- , and MA^+ are shown as gray, yellow, and blue atoms, respectively. (b) The electron and hole radial probability distribution under different types of lattice screenings from path integral simulations. Reproduced with permission from ref 15. Copyright 2022 American Chemical Society.

III.C. Radiative Recombination in Nanocrystals

The optoelectronic properties of nanocrystals depend intricately on both size-dependent quantum confinement and lattice symmetry. When a photogenerated electron–hole pair forms, its spatial extent, characterized by the exciton Bohr radius, determines how confinement affects the excitonic behavior. In nanocrystals of a radius smaller than the Bohr radius, the exciton is confined within the nanocrystal volume, leading to discrete energy levels and size-tunable radiative recombination. These recombination dynamics are further modulated by the underlying lattice symmetry.^{3,56} Room temperature photoluminescence measurements of perovskite nanocrystals reveal fast radiative recombination on a nanosecond time scale with near-unity photoluminescence quantum yield, indicating possible applications in quantum light generation.³ Recent studies of size-dependent radiative rates in confined nanocrystals have revealed a nonmonotonic trend in exciton radiative recombination for CsPbBr_3 nanocrystals, with peak rates observed for nanocrystals around 5.5 nm in size, corresponding to an intermediate confinement regime. This nonmonotonic behavior is most pronounced in structures distorted away from cubic symmetry due to modification of the exciton level structure under reduced lattice symmetry.⁵⁵ Thus, a detailed understanding of how quantum confinement and lattice distortion influence radiative recombination is necessary for designing optimal platforms for perovskite nanocrystal-based optical devices.

To elucidate the interplay of structural and electronic effects, we combined molecular dynamics simulations for lattice

dynamics with atomistic semiempirical pseudopotential calculations for excitonic states. The detailed theoretical framework has been described elsewhere.^{22,24} A size-dependent transition was found in agreement with previous work,²² where small, approximately 2 nm CsPbX_3 cubes are cubic and larger, > 4 nm CsPbX_3 nanocrystals ($X = \text{I}, \text{Br}$) have increased lattice distortion toward the orthorhombic geometry. Atomistic pseudopotential + BSE calculations were carried out for lead halide perovskite nanocrystals ranging from 2 to 7 nm in size, considering three structural symmetries: ideal cubic, orthorhombic, and force-field-relaxed geometries. The computed energies and oscillator strengths were fitted to extrapolate the radiative rate at larger nanocrystal sizes. Boltzmann thermal averaged radiative rates were computed in the time-dependent perturbation theory framework as

$$\langle k_r \rangle = \left[\sum_n e^{-\beta \hbar \omega_n} \frac{\omega_n^3 |\mu_n|^2}{3\pi \epsilon_0 \hbar c^3} \right] / \sum_n e^{-\beta \hbar \omega_n} \quad (6)$$

where μ_n and ω_n are the oscillator strength and Bohr frequency of exciton n , ϵ_0 is the permittivity of free space, and c is the speed of light. Radiative rates, which are in good agreement with experimental measurements,⁵⁵ are proportional to the exciton oscillator strength, which increases with nanocrystal size due to the larger electron–hole overlap in the nanocrystal volume. From this trend, it is expected that the radiative rates increase monotonically for larger nanocrystals. However, as shown in Figure 7(a), the radiative rates increase between 2 and 5 nm, which we attribute to a size-dependent increase in the oscillator strength of the lowest bright exciton state, as shown in Figure 7(b). This trend is observed irrespective of crystal symmetry. However, this increase in oscillator strength does not continue to reduce the radiative lifetime in larger nanocrystals approaching the weak confinement regime, consistent with experimental trends. Instead, as nanocrystal size increases, the growing density of states enables thermal population of higher-lying, low oscillator strength “dim” exciton states. This thermal redistribution reduces the Boltzmann population of the lowest bright triplet manifold, Figure 7(c), leading to longer radiative lifetimes despite stronger individual transitions. These dim states exhibit an equilibrium population distribution due to the long, nanosecond time scale of radiative recombination compared to the picosecond hot exciton cooling rates. This thermal redistribution reduces the Boltzmann population of the lowest bright triplet manifold, leading to longer radiative lifetimes despite stronger individual transitions. The observed non-monotonic radiative rates emerge distinctly in orthorhombic and relaxed nanocrystals of lowered structural symmetry due to exciton level splitting that simultaneously reduces the energy gap from the bright to dim states and increases the density of the lower energy dim states; cubic nanocrystals are not predicted to show nonmonotonic radiative rates.

III.D. Phonon Dephasing

The relaxation of excited charges proceeds through charge-phonon interactions, exciting lattice vibrations that themselves must subsequently relax. The examination of the dynamics of the lattice vibrations that charges are coupled to can thus provide insight into the behavior of excited states and clarify the ways in which they are coupled. In layered perovskites, experimental observations have reported rich lattice dynamics owing to their ionic inorganic framework together with the

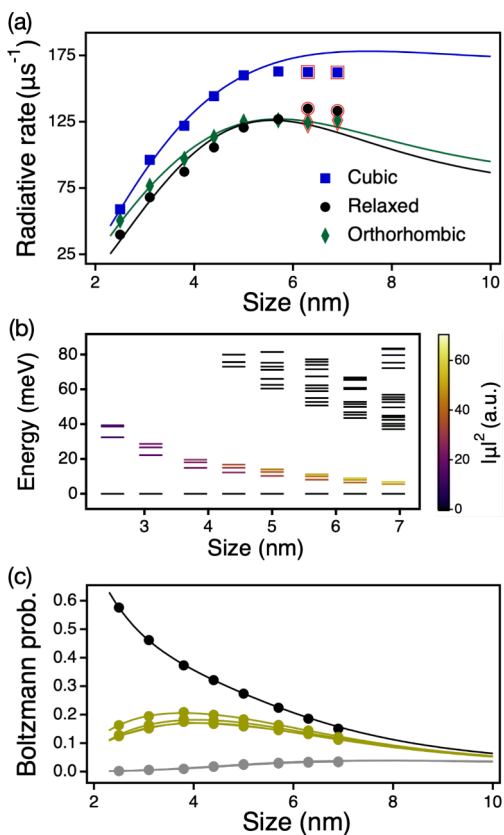


Figure 7. (a) Size-dependent radiative recombination rates show nonmonotonicity due to the increasing oscillator strength for larger nanocrystals in competition with increasing thermal population of higher energy, dim excitonic states. Points represent rates calculated on atomistic nanocrystal structures, and the lines represent radiative rates predicted from fits of exciton energies and oscillator strengths without direct fitting to the rate data. The red-ringed points are test points and were not included in the fitting data. (b) Representative exciton energy level diagram for orthorhombic CsPbI_3 nanocrystals of different edge lengths. The color indicates the squared transition dipole magnitude of the exciton. (c) Size-dependent Boltzmann probabilities for the lowest exciton (black), bright triplets (gold), and dim states (gray) of orthorhombic CsPbI_3 show nonmonotonicity due to the thermal population of higher-lying states at larger sizes. Reproduced with permission from ref 55. Copyright 2025 Nature.

softness arising from the organic barrier layers. Early work by Quan et al. reported the dependence of photoluminescence quantum yield on the organic ligand environments.¹² They observed that layered perovskites with aromatic organic groups show much higher yields compared to those with alkyl groups. Delving into the role of dynamics of the lattice, with pump-probe spectroscopy (illustrated in Figure 8(a)), vibrational relaxation dynamics were studied through phonon dephasing rate with mainly two different organic ligands, *n*-butylamine (BTA) and phenylethylamine (PEA). It was found that phonon relaxation with BTA ligands is much faster than with PEA ligands. While with the faster dephasing rate over the range of temperature, contrary to the prediction from a general scattering theory,⁵⁷ the dephasing rates of BTA ligands exhibit no temperature dependence whereas the rates from PEA ligands show a linear temperature dependence. Hence, these distinct dynamics, depending on the organic ligands given the same inorganic framework, indicate the importance of the

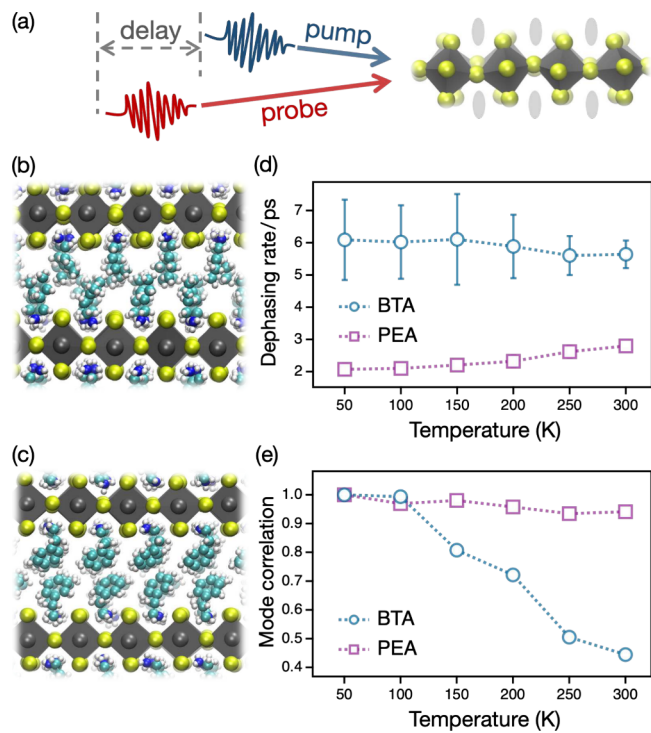


Figure 8. (a) Schematic illustration of transient pump–probe measurement (absorption spectroscopy) on two-dimensional layered perovskites. (b, c) Snapshots of molecular dynamics simulations on (b) $(\text{BTA})_2\text{PbBr}_4$ and (c) $(\text{PEA})_2\text{PbBr}_4$ layered perovskites, respectively. (d) Phonon dephasing rate of the lowest optical mode with BTA (blue circles) and PEA (purple squares) organic ligands. (e) Correlation between lowest frequency optical modes at different temperatures. Dotted lines are guides to the eye. Reproduced with permission from ref 12. Copyright 2021 National Academy of Sciences.

organic ligands in describing lattice dynamics in layered perovskites.

To obtain a molecular level understanding of vibrational dynamics of layered perovskites, molecular dynamics simulations⁵⁸ were performed. While simple, the basic physical properties such as lattice constants and mechanical properties were reasonably reproduced by the model whose simulation snapshots with BTA and PEA ligands are shown in Figure 8(b) and (c), respectively. To effectively extract the phonon modes, the fluctuation–dissipation theorem is employed to relate displacement correlations from simulations to the dynamical matrix⁵⁹ where the analysis on the resultant vibrational frequencies and phonon modes verifies that the organic ligands largely participate in forming vibrational modes in layered perovskites.¹²

For the lowest frequency optical mode, the atomistic model qualitatively captured the phonon dephasing dynamics observed experimentally in each layered perovskites. In the classical limit, derived from the Fermi's golden rule, the relaxation rate of vibrational mode λ can be computed from the Fourier transform of the corresponding force–force correlation function⁶⁰ as

$$\Gamma_\lambda = \frac{1}{k_B T} \int_0^\infty dt \cos(\omega_\lambda t) \langle F_\lambda(0) F_\lambda(t) \rangle \quad (7)$$

where ω_λ is the optical frequency and F_λ is the mass-weighted force exerted on mode λ due to the coupling with their

surrounding lattice. Figure 8(d) describes the dephasing rate in BTA and PEA layered perovskites over a range of temperatures, showing that the dephasing rates of BTA layered perovskite are higher than the one from PEA layered perovskite and are insensitive to the temperature.

Different phonon dynamics in layered perovskites were understood by comparing their packing geometry and anharmonicity of the organic ligands. As deduced from Figure 8(b) and (c), compared to PEA ligands where molecules are well aligned via strong π - π interaction, BTA ligands hold amorphous packing geometry even at low temperature, whose dynamic disorder can rationalize the temperature insensitive relaxation rate. In terms of the higher rate of BTA perovskites, this can be resolved by the large anharmonicity of BTA ligands. Based on the structural analysis of organic ligands, the local potential associated with the ligand orientation turns out to be highly anharmonic in BTA perovskite, showing a large deviation from the prediction based on fluctuation–dissipation theorem (see ref 12 for the detailed analysis). This is further supported by calculations showing the correlation between optical modes at different temperatures, described in Figure 8(e) where the value ranges from 0 to 1 with value 1 indicating that two vibrational modes are identical. While for PEA perovskites, the values are close to 1 across the whole range of temperature, the large drop in BTA perovskites as increasing the temperature implies that the optical modes are highly mixed with increasing temperature, a signal of large anharmonicity. An Umklapp scattering model employed in ref 12 demonstrated that the dominant decay pathway for each optical mode was to two acoustic modes.

IV. CONCLUDING REMARKS

In this Account, we have outlined our studies describing the effects of the perovskite lattice on the excited state properties. For both static and dynamic properties, while various computational and analytical descriptions for excited states and lattices are considered in our approaches presented here, our focus has been on how to include the lattice effect and how important it is. Our calculations confirm that the lattice distortion resulting from the structural relaxation needs to be considered to properly describe the electronic states in perovskites. Further, it is found that the lattice fluctuations affect phonon dynamics itself and also dynamics of charge carriers, generically reducing the mobility, exciton binding energy, and electron–hole recombination rate, whereas there are negligible effects on biexciton bindings. We expect these results along with the strategic approaches to drive the continued exploration on the role of lattice effects in elucidating the origin of how the lattice renormalizes excited state properties in lead halide perovskites.

■ AUTHOR INFORMATION

Corresponding Author

David T. Limmer — Department of Chemistry, University of California, Berkeley, California 94720, United States; Materials Science Division and Chemical Science Division, Lawrence Berkeley National Laboratory, Berkeley, California 94720, United States; Kavli Energy NanoScience Institute, Berkeley, California 94720, United States;  orcid.org/0000-0002-2766-0688; Email: dlimmer@berkeley.edu

Authors

Yoonjae Park — Department of Chemistry, University of California, Berkeley, California 94720, United States; Materials Science Division, Lawrence Berkeley National Laboratory, Berkeley, California 94720, United States;  orcid.org/0000-0002-7893-3076

Rohit Rana — Department of Chemistry, University of California, Berkeley, California 94720, United States; Materials Science Division, Lawrence Berkeley National Laboratory, Berkeley, California 94720, United States;  orcid.org/0000-0001-6389-1419

Daniel Chabeda — Department of Chemistry, University of California, Berkeley, California 94720, United States;  orcid.org/0000-0003-0152-7528

Eran Rabani — Department of Chemistry, University of California, Berkeley, California 94720, United States; Materials Science Division, Lawrence Berkeley National Laboratory, Berkeley, California 94720, United States; The Sackler Center for Computational Molecular and Materials Science, Tel Aviv University, Tel Aviv 69978, Israel;  orcid.org/0000-0003-2031-3525

Complete contact information is available at:
<https://pubs.acs.org/10.1021/accountsrm.4c00401>

Notes

The authors declare no competing financial interest.

Biographies

Yoonjae Park received her B.S. in Chemistry and Mathematics and M.S. in Chemistry from Sogang University (South Korea) in 2016 and 2018, respectively. She obtained her Ph.D. in Chemistry from the University of California, Berkeley, under the supervision of Prof. David Limmer in 2023. She is currently a postdoctoral researcher in the Department of Chemistry at Massachusetts Institute of Technology, working with Prof. Adam Willard.

Rohit Rana is currently a graduate student at the University of California, Berkeley. He obtained his B.S. from the University of Florida in Chemistry, Mathematics, and Statistics in 2021. His current research interests are in studying exciton binding and dynamics in novel semiconductors.

Daniel Chabeda received his B.S. in chemistry from Yale University in 2022. He is now pursuing PhD studies at the University of California at Berkeley, where he is advised by Eran Rabani and supported by the National Science Foundation Graduate Research Fellowship Program. His research explores electronic structure and dynamics at the nanoscale, with specific focus on chiroptical phenomena and exciton relaxation in perovskite nanocrystals.

Eran Rabani completed his B.Sc. and Ph.D. at the Hebrew University. After his postdoctoral work at Columbia University, he became a faculty member at Tel Aviv University. In 2014, he joined the University of California, Berkeley, where he holds the Glenn T. Seaborg Chair in Physical Chemistry. He is also a faculty member at Lawrence Berkeley National Laboratory. His research focuses on advancing the understanding of nanostructures through theoretical models and simulations, covering phenomena such as self-assembly, phase transitions, excitonic and multiexcitonic dynamics, electron transfer processes, and other complex behaviors in nanoscale systems.

David T. Limmer David Limmer received his B.S. in chemical engineering in 2008 from the New Mexico Institute of Mining and Technology, and his Ph.D. in chemistry from the University of California, Berkeley under the supervision of David Chandler. From

2013–2016, David was an independent fellow of the Princeton Center for Theoretical Science. In 2016, he joined the faculty of the Department of Chemistry at the University of California, Berkeley, and holds appointments as a Research Scientist in the Materials and Chemical Sciences Divisions of Lawrence Berkeley National Laboratory, and a Fellow of the Kavli Energy NanoSciences Institute. His research focuses on the molecular dynamics of condensed phase systems, especially in instances where near-equilibrium principles do not apply.

ACKNOWLEDGMENTS

Support for this work was provided by the U.S. Department of Energy, Office of Science, Office of Basic Energy Sciences, Materials Sciences and Engineering Division, under Contract No. DEAC02-05-CH11231 within the Fundamentals of Semiconductor Nanowire Program (KCPY23). Computational resources were provided in part by the National Energy Research Scientific Computing Center (NERSC), a U.S. Department of Energy Office of Science User Facility operated under contract no. DEAC02-05CH11231. This material is based upon work supported by the National Science Foundation Graduate Research Fellowship Program under Grant No. DGE 2146752 (DC). Any opinions, findings, and conclusions or recommendations expressed in this material are those of the author(s) and do not necessarily reflect the views of the National Science Foundation. We would like to thank other collaborators who participated in the work reviewed here including Amael Obliger, Daniel Weinberg, Peidong Yang, and Paul Alivisatos.

REFERENCES

- (1) Zhu, X.-Y.; Podzorov, V. Charge Carriers in Hybrid Organic-Inorganic Lead Halide Perovskites Might Be Protected as Large Polarons. *J. Phys. Chem. Lett.* **2015**, *6*, 4758–4761.
- (2) Miyata, K.; Meggiolaro, D.; Trinh, M. T.; Joshi, P. P.; Mosconi, E.; Jones, S. C.; Angelis, F. D.; Zhu, X.-Y. Large polarons in lead halide perovskites. *Science Advances* **2017**, *3*, e1701217.
- (3) Kovalenko, M. V.; Protesescu, L.; Bodnarchuk, M. I. Properties and potential optoelectronic applications of lead halide perovskite nanocrystals. *Science* **2017**, *358*, 745–750.
- (4) Herz, L. M. Charge-carrier dynamics in organic-inorganic metal halide perovskites. *Annu. Rev. Phys. Chem.* **2016**, *67*, 65–89.
- (5) de Quilettes, D. W.; Vorpahl, S. M.; Stranks, S. D.; Nagaoka, H.; Eperon, G. E.; Ziffer, M. E.; Snaith, H. J.; Ginger, D. S. Impact of microstructure on local carrier lifetime in perovskite solar cells. *Science* **2015**, *348*, 683–686.
- (6) Wehrenfennig, C.; Eperon, G. E.; Johnston, M. B.; Snaith, H. J.; Herz, L. M. High Charge Carrier Mobilities and Lifetimes in Organolead Trihalide Perovskites. *Adv. Mater.* **2014**, *26*, 1584–1589.
- (7) Wang, H.; Valkunas, L.; Cao, T.; Whittaker-Brooks, L.; Fleming, G. R. Coulomb Screening and Coherent Phonon in Methylammonium Lead Iodide Perovskites. *J. Phys. Chem. Lett.* **2016**, *7*, 3284–3289.
- (8) Fröhlich, H. Electrons in lattice fields. *Adv. Phys.* **1954**, *3*, 325–361.
- (9) Devreese, J. T. Fröhlich Polarons. Lecture course including detailed theoretical derivations. *arXiv*, 1012.4576, 2015.
- (10) Chen, Y.; Yi, H. T.; Wu, X.; Haroldson, R.; Gartstein, Y. N.; Rodionov, Y. I.; Tikhonov, K. S.; Zakhidov, A.; Zhu, X. Y.; Podzorov, V. Extended carrier lifetimes and diffusion in hybrid perovskites revealed by Hall effect and photoconductivity measurements. *Nat. Commun.* **2016**, *7*, 12253.
- (11) Limmer, D. T.; Ginsberg, N. S. Photoinduced phase separation in the lead halides is a polaronic effect. *J. Chem. Phys.* **2020**, *152*, 230901.
- (12) Quan, L. N.; Park, Y.; Guo, P.; Gao, M.; Jin, J.; Huang, J.; Copper, J. K.; Schwartzberg, A.; Schaller, R.; Limmer, D. T.; Yang, P. Vibrational relaxation dynamics in layered perovskite quantum wells. *Proc. Natl. Acad. Sci. U. S. A.* **2021**, *118*, e2104425118.
- (13) Schlipf, M.; Poncée, S.; Giustino, F. Carrier Lifetimes and Polaronic Mass Enhancement in the Hybrid Halide Perovskite CH₃NH₃PbI₃ from Multiphonon Fröhlich Coupling. *Phys. Rev. Lett.* **2018**, *121*, 086402.
- (14) Mayers, M. Z.; Tan, L. Z.; Egger, D. A.; Rappe, A. M.; Reichman, D. R. How lattice and charge fluctuations control carrier dynamics in halide perovskites. *Nano Lett.* **2018**, *18*, 8041–8046.
- (15) Park, Y.; Obliger, A.; Limmer, D. T. Nonlocal Screening Dictates the Radiative Lifetimes of Excitations in Lead Halide Perovskites. *Nano Lett.* **2022**, *22*, 2398–2404.
- (16) Park, Y.; Limmer, D. T. Renormalization of excitonic properties by polar phonons. *J. Chem. Phys.* **2022**, *157*, 104116.
- (17) Rabani, E.; Hetényi, B.; Berne, B. J.; Brus, L. E. Electronic properties of CdSe nanocrystals in the absence and presence of a dielectric medium. *J. Chem. Phys.* **1999**, *110*, 5355–5369.
- (18) Zhao, Q.; Hazarika, A.; Schellhas, L. T.; Liu, J.; Gaulding, E. A.; Li, G.; Zhang, M.; Toney, M. F.; Sercel, P. C.; Luther, J. M. Size-Dependent Lattice Structure and Confinement Properties in CsPbI₃ Perovskite Nanocrystals: Negative Surface Energy for Stabilization. *ACS Energy Letters* **2020**, *5*, 238–247.
- (19) Rainò, G.; Landuyt, A.; Krieg, F.; Bernasconi, C.; Ochsenbein, S. T.; Dirin, D. N.; Bodnarchuk, M. I.; Kovalenko, M. V. Underestimated Effect of a Polymer Matrix on the Light Emission of Single CsPbBr₃ Nanocrystals. *Nano Lett.* **2019**, *19*, 3648–3653.
- (20) Becker, M. A.; Vaxenburg, R.; Nedelcu, G.; Sercel, P. C.; Shabaev, A.; Mehl, M. J.; Michopoulos, J. G.; Lambrakos, S. G.; Bernstein, N.; Lyons, J. L.; Stöferle, T.; Mahrt, R. F.; Kovalenko, M. V.; Norris, D. J.; Rainò, G.; Efros, A. L. Bright triplet excitons in caesium lead halide perovskites. *Nature* **2018**, *553*, 189–193.
- (21) Swift, M. W.; Sercel, P. C.; Efros, A. L.; Lyons, J. L.; Norris, D. J. Identification of Semiconductor Nanocrystals with Bright Ground-State Excitons. *ACS Nano* **2024**, *18*, 19561–19567.
- (22) Weinberg, D.; Park, Y.; Limmer, D. T.; Rabani, E. Size-Dependent Lattice Symmetry Breaking Determines the Exciton Fine Structure of Perovskite Nanocrystals. *Nano Lett.* **2023**, *23*, 4997–5003.
- (23) Dastidar, S.; Hawley, C. J.; Dillon, A. D.; Gutierrez-Perez, A. D.; Spanier, J. E.; Fafarman, A. T. Quantitative Phase-Change Thermodynamics and Metastability of Perovskite-Phase Cesium Lead Iodide. *J. Phys. Chem. Lett.* **2017**, *8*, 1278–1282.
- (24) Bischak, C. G.; Lai, M.; Fan, Z.; Lu, D.; David, P.; Dong, D.; Chen, H.; Etman, A. S.; Lei, T.; Sun, J.; Gränwald, M.; Limmer, D. T.; Yang, P.; Ginsberg, N. S. Liquid-like Interfaces Mediate Structural Phase Transitions in Lead Halide Perovskites. *Matter* **2020**, *3*, 534–545.
- (25) Filip, M. R.; Haber, J. B.; Neaton, J. B. Phonon Screening of Excitons in Semiconductors: Halide Perovskites and Beyond. *Phys. Rev. Lett.* **2021**, *127*, 067401.
- (26) Umari, P.; Mosconi, E.; Angelis, F. D. Infrared Dielectric Screening Determines the Low Exciton Binding Energy of Metal-Halide Perovskites. *J. Phys. Chem. Lett.* **2018**, *9*, 620–627.
- (27) Pollmann, J.; Büttner, H. Effective Hamiltonians and binding energies of Wannier excitons in polar semiconductors. *Phys. Rev. B* **1977**, *16*, 4480.
- (28) Sun, S.; Salim, T.; Mathews, N.; Duchamp, M.; Boothroyd, C.; Xing, G.; Sum, T. C.; Lam, Y. M. The origin of high efficiency in low-temperature solution-processable bilayer organometal halide hybrid solar cells. *Energy Environ. Sci.* **2014**, *7*, 399–407.
- (29) Saba, M.; Cadelano, M.; Marongiu, D.; Chen, F.; Sarritzu, V.; Sestu, N.; Figus, C.; Aresti, M.; Piras, R.; Lehmann, A. G.; Cannas, C.; Musinu, A.; Quochi, F.; Mura, A.; Bongiovanni, G. Correlated electron–hole plasma in organometal perovskites. *Nat. Commun.* **2014**, *5*, 5049.
- (30) Sestu, N.; Cadelano, M.; Sarritzu, V.; Chen, F.; Marongiu, D.; Piras, R.; Mainas, M.; Quochi, F.; Saba, M.; Mura, A.; Bongiovanni, G.

- Absorption F-Sum Rule for the Exciton Binding Energy in Methylammonium Lead Halide Perovskites. *J. Phys. Chem. Lett.* **2015**, *6*, 4566–4572.
- (31) Feynman, R. P. *Statistical Mechanics*; Westview, 1998.
- (32) Feynman, R. P.; Hibbs, A. R. *Quantum Mechanics and Path Integrals*; Dover, 2005.
- (33) Chandler, D.; Wolynes, P. G. Exploiting the isomorphism between quantum theory and classical statistical mechanics of polyatomic fluids. *J. Chem. Phys.* **1981**, *74*, 4078–4095.
- (34) Ceperley, D. M. Path integrals in the theory of condensed helium. *Rev. Mod. Phys.* **1995**, *67*, 279.
- (35) Mattoni, A.; Filippetti, A.; Caddeo, C. Modeling hybrid perovskites by molecular dynamics. *J. Phys.: Condens. Matter* **2017**, *29*, 043001.
- (36) Alexandrov, A. S.; Devreese, J. T. *Advances in polaron physics*; Springer, 2010; Vol. 159.
- (37) Galkowski, K.; Mitioglu, A.; Miyata, A.; Plochocka, P.; Portugall, O.; Eperon, G. E.; Wang, J. T.-W.; Stergiopoulos, T.; Stranks, S. D.; Snaith, H. J.; Nicholas, R. J. Determination of the exciton binding energy and effective masses for methylammonium and formamidinium lead tri-halide perovskite semiconductors. *Energy Environ. Sci.* **2016**, *9*, 962–970.
- (38) Blancon, J.-C.; Stier, A. V.; Tsai, H.; Nie, W.; Stoumpos, C. C.; Traoré, B.; Pedesseau, L.; Kepenekian, M.; Katsutani, F.; Noe, G. T.; Kono, J.; Tretiak, S.; Crooker, S. A.; Katan, C.; Kanatzidis, M. G.; Crochet, J. J.; Even, J.; Mohite, A. D. Scaling law for excitons in 2D perovskite quantum wells. *Nat. Commun.* **2018**, *9*, 2254.
- (39) Delport, G.; Chehade, G.; Lédée, F.; Diab, H.; Milesi-Brault, C.; Trippé-Allard, G.; Even, J.; Lauret, J.-S.; Deleporte, E.; Garrot, D. Exciton-exciton annihilation in two-dimensional halide perovskites at room temperature. *J. Phys. Chem. Lett.* **2019**, *10*, 5153–5159.
- (40) Urban, J. M.; Chehade, G.; Dyksik, M.; Menahem, M.; Surrenta, A.; Trippé-Allard, G.; Maude, D. K.; Garrot, D.; Yaffe, O.; Deleporte, E.; Plochocka, P.; Baranowski, M. Revealing Excitonic Phonon Coupling in $(\text{PEA})_2(\text{MA})_{n-1}\text{Pb}_n\text{I}_{3n+1}$ 2D Layered Perovskites. *J. Phys. Chem. Lett.* **2020**, *11*, 5830–5835.
- (41) Rana, R.; Limmer, D. T. On the interplay of electronic and lattice screening on exciton binding in two-dimensional lead halide perovskites. *Nano Lett.* **2025**, *25*, 4727–4733.
- (42) Tyagi, D.; Laxmi, V.; Basu, N.; Reddy, L.; Tian, Y.; Ouyang, Z.; Nayak, P. K. Recent advances in two-dimensional perovskite materials for light-emitting diodes. *Discover Nano* **2024**, *19*, 109.
- (43) Hanamura, E.; Nagaosa, N.; Kumagai, M.; Takagahara, T. Quantum wells with enhanced exciton effects and optical nonlinearity. *Materials Science and Engineering: B* **1988**, *1*, 255–258.
- (44) Sio, W. H.; Giustino, F. Unified ab initio description of Fröhlich electron-phonon interactions in two-dimensional and three-dimensional materials. *Phys. Rev. B* **2022**, *105*, 115414.
- (45) Zhu, C.; Nguyen, T.; Boehme, S. C.; Moskalenko, A.; Dirin, D. N.; Bodnarchuk, M. I.; Katan, C.; Even, J.; Rainò, G.; Kovalenko, M. V. Many-Body Correlations and Exciton Complexes in CsPbBr₃ Quantum Dots. *Adv. Mater.* **2023**, *35*, 2208354.
- (46) Dana, J.; Binyamin, T.; Etgar, L.; Ruhman, S. Unusually Strong Biexciton Repulsion Detected in Quantum Confined CsPbBr₃ Nanocrystals with Two and Three Pulse Femtosecond Spectroscopy. *ACS Nano* **2021**, *15*, 9039.
- (47) Lubin, G.; Tenne, R.; Ulku, A. C.; Antolovic, I. M.; Burri, S.; Karg, S.; Yallapragada, V. J.; Bruschini, C.; Charbon, E.; Oron, D. Heralded Spectroscopy Reveals Exciton–Exciton Correlations in Single Colloidal Quantum Dots. *Nano Lett.* **2021**, *21*, 6756–6763.
- (48) Cho, K.; Yamada, T.; Tahara, H.; Tadano, T.; Suzuura, H.; Saruyama, M.; Sato, R.; Teranishi, T.; Kanemitsu, Y. Luminescence Fine Structures in Single Lead Halide Perovskite Nanocrystals: Size Dependence of the Exciton-Phonon Coupling. *Nano Lett.* **2021**, *21*, 7206–7212.
- (49) Brennan, M. C.; Forde, A.; Zhukovsky, M.; Baublis, A. J.; Morozov, Y. V.; Zhang, S.; Zhang, Z.; Kilin, D. S.; Kuno, M. Universal Size-Dependent Stokes Shifts in Lead Halide Perovskite Nanocrystals. *J. Phys. Chem. Lett.* **2020**, *11*, 4937–4944.
- (50) Park, Y.; Limmer, D. T. Biexcitons are bound in CsPbBr₃ perovskite nanocrystals. *Physical Review Materials* **2023**, *7*, 106002.
- (51) Li, Z.; Wei, Q.; Wang, Y.; Tao, C.; Zou, Y.; Liu, X.; Li, Z.; Wu, Z.; Li, M.; Guo, W.; Li, G.; Xu, W.; Gao, F. Highly bright perovskite light-emitting diodes enabled by retarded Auger recombination. *Nat. Commun.* **2025**, *16*, 927.
- (52) Martin, B. A. A.; Frost, J. M. Multiple phonon modes in Feynman path-integral variational polaron mobility. *Phys. Rev. B* **2023**, *107*, 115203.
- (53) Kornilovitch, P. E. Continuous-Time Quantum Monte Carlo Algorithm for the Lattice Polaron. *Phys. Rev. Lett.* **1998**, *81*, 5382–5385.
- (54) Marshall, J. T.; Chawla, M. S. Feynman Path-Integral Calculation of the Polaron Effective Mass. *Phys. Rev. B* **1970**, *2*, 4283–4287.
- (55) Abbas, A. S.; Chabeda, D.; Weinberg, D.; Limmer, D. T.; Rabani, E.; Alivisatos, A. P. Non-Monotonic size-dependent exciton radiative lifetime in CsPbBr₃ Nanocrystals. *Nat. Commun.* **2025**, *16*, 6401.
- (56) Alivisatos, A. Semiconductor clusters, nanocrystals, and quantum dots. *Science* **1996**, *271*, 933–937.
- (57) Verma, P.; Abbi, S. C.; Jain, K. P. Raman-scattering probe of anharmonic effects in GaAs. *Phys. Rev. B* **1995**, *51*, 16660–16667.
- (58) Hata, T.; Giorgi, G.; Yamashita, K.; Caddeo, C.; Mattoni, A. Development of a Classical Interatomic Potential for MAPbBr₃. *J. Phys. Chem. C* **2017**, *121*, 3724–3733.
- (59) Kong, L. T. Phonon dispersion measured directly from molecular dynamics simulations. *Comput. Phys. Commun.* **2011**, *182*, 2201–2207.
- (60) Egorov, S.; Everitt, K.; Skinner, J. Quantum dynamics and vibrational relaxation. *J. Phys. Chem. A* **1999**, *103*, 9494–9499.



CAS BIOFINDER DISCOVERY PLATFORM™

PRECISION DATA FOR FASTER DRUG DISCOVERY

CAS BioFinder helps you identify targets, biomarkers, and pathways

Unlock insights

CAS
A division of the American Chemical Society